

## Measuring the transverse magnetization of rotating ferrofluids

J. P. Embs,<sup>1,2,\*</sup> S. May,<sup>3,4</sup> C. Wagner,<sup>3</sup> A. V. Kityk,<sup>5</sup> A. Leschhorn,<sup>2</sup> and M. Lücke<sup>2</sup>

<sup>1</sup>*Technische Physik, Universität des Saarlandes, 66041 Saarbrücken, Germany*

<sup>2</sup>*Theoretische Physik, Universität des Saarlandes, 66041 Saarbrücken, Germany*

<sup>3</sup>*Experimentalphysik, Universität des Saarlandes, 66041 Saarbrücken, Germany*

<sup>4</sup>*Department of Physics, University of Hull, HU6 7RX, United Kingdom*

<sup>5</sup>*Institute for Computer Science, Electrical Engineering Department, Technical University of Czestochowa, Al. Armii Krajowej 17, PL-42200, Czestochowa, Poland*

(Received 19 August 2005; published 2 March 2006)

We report on measurements of the transverse magnetization of a ferrofluid rotating as a rigid body in a constant magnetic field,  $\mathbf{H}_0$ , applied perpendicular to the axis of rotation. The rotation of the fluid leads to a nonequilibrium situation, where the ferrofluid magnetization  $\mathbf{M}$  and the magnetic field within the sample,  $\mathbf{H}$ , are no longer parallel to each other. The off-axis magnetization perpendicular to  $\mathbf{H}_0$  is measured as a function of both the applied magnetic field  $H_0$  and the angular frequency  $\Omega$ . The latter ranges from a few hertz to frequencies well above a characteristic inverse Brownian relaxation time. Our experimental results strongly indicate that the transverse magnetization is caused only by a small fraction of the colloidal ferromagnetic particles. The effect of the polydispersity of the ferrofluid is discussed. Experimental results are compared to predictions based on several theoretical models. A single-time relaxation approach for the so-called effective field and a field-dependent Debye relaxation of  $\mathbf{M}$  yield reasonably good shapes of the curves of transverse magnetization vs  $\Omega$ . However, like the other models, they overestimate their magnitudes.

DOI: [10.1103/PhysRevE.73.036302](https://doi.org/10.1103/PhysRevE.73.036302)

PACS number(s): 47.32.-y, 47.65.-d

### I. INTRODUCTION

Ferrofluids are colloidal suspensions containing monodomain ferro- or ferrimagnetic nanoparticles with a typical diameter of 10 nm [1]. Each particle carries a permanent magnetic moment, which is proportional to the volume of its magnetic core. To suppress agglomeration, the particles in the ferrofluids that have been investigated are covered with a surfactant coating, which prevents them from approaching each other too closely. The hydrodynamic diameter  $d_h$  of these particles (magnetic core plus dead layer plus surfactant coating) has a significant influence on the interaction between the particles and the carrier liquid. Many phenomena in ferrofluids, such as the viscosity enhancement in a static magnetic field [2,3], the occurrence of “negative viscosity” [4–6], or the magnetovortical resonance [7,8], are direct results of this interaction. Nowadays, ferrofluids are used in a broad range of applications from vacuum seals to medical treatments [1,9,10]. But despite a long research history, there is yet no full understanding of the dynamics of ferrofluids. In particular, a generally accepted constitutive equation is still missing. It is therefore reasonable to investigate a key mechanism of ferrofluids carefully, namely, the difference of rotation of the suspended particles and the surrounding carrier liquids in a constant external magnetic field.

Heegaard *et al.* [7], and Gazeau *et al.* [11] used magneto-optical birefringence to examine the local vorticity  $\Omega$  of dilute ferrofluid flow. While they measured the angle between  $\mathbf{H}$  and  $\mathbf{M}$  by means of optical birefringence in a dilute ferrofluid sample, the subject to our research is to measure the

same effect via the off-axis magnetization component in a nondilute ferrofluid. In Heegaard *et al.*'s work [7], the rotation rate varies between zero and 220 rad/s. They present data of the normalized birefringence intensity as function of  $\Omega$ . However, the frequency range was too small to allow for the observation of a peak behavior as a function of  $\Omega$  that is predicted by many theoretical models for the magnetization dynamics. Furthermore, since only a normalized quantity was reported, a direct quantitative comparison to theoretical predictions is not possible.

Some of the coauthors of this work used a torsional pendulum [12] in order to examine the transverse relaxation time  $\tau_{\perp}(H_0)$  and the rotational viscosity  $\eta_R(H_0)$  in the shear-free flow of rigid-body rotation (RBR) as function of the externally applied magnetic field  $H_0$ . The torsional pendulum experiment [12] was operated by necessity in the low-frequency regime  $\Omega\tau \ll 1$ , where  $\tau$  denotes the relaxation time of the relevant relaxation process. To obtain a more complete insight into the rotational dynamics of ferrofluids we have devised an experiment that can probe also higher frequencies. For that purpose we use a slender cylinder filled with ferrofluid in a spatially homogeneous constant magnetic field perpendicular to the cylinder axis. The cylinder with the ferrofluid is rotating as a rigid body with constant frequency. Within this experiment, the rotation rate  $\Omega$  is varied between zero and 2500 rad/s and thus extends well into a range where  $\Omega\tau \geq 1$ .

In the rotating ferrofluid, the local magnetization  $\mathbf{M}(\mathbf{r}, t)$  will be off from the equilibrium value  $\mathbf{M}_{\text{eq}}(H)$  and a viscous-drag torque occurs by virtue of the difference between the angular velocity of the particles and the local angular velocity of the surrounding liquid. In order to countervail this flow-induced torque, a magnetic torque  $\mathbf{M} \times \mathbf{H}$  appears. This

\*Electronic address: [jp.embs@mx.uni-saarland.de](mailto:jp.embs@mx.uni-saarland.de)

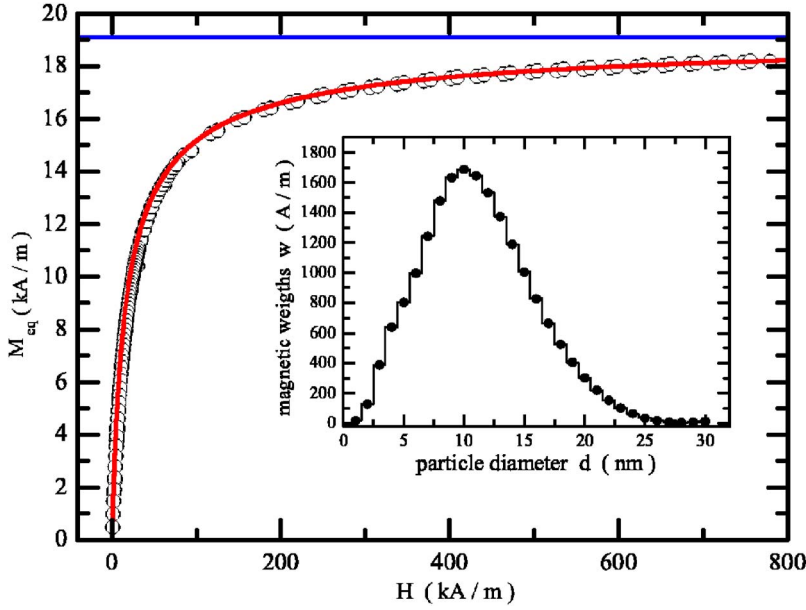


FIG. 1. (Color online) Equilibrium magnetization  $M_{\text{eq}}$  as function of the internal field  $H$  for the ferrofluid AGP 933 of FerroTec. The horizontal line marks the saturation magnetization  $M_{\text{sat}}^{\text{FF}} = 19\,108.6$  A/m. The inset shows the distribution of the magnetic weights  $w$  as function of the magnetic particle diameter  $d$  (in nanometers) as deduced from  $M_{\text{eq}}(H)$  using Tichonovs regularization method.

interplay between the flow-induced and the magnetic torque generates a component of  $\mathbf{M}$  perpendicular to the externally applied field  $\mathbf{H}_0$ . Deviations from the equilibrium are largest when the rotation rate  $\Omega$  of the fluid is comparable to the relaxation rate  $1/\tau$ .

According to Maxwell's equations, the relation between the constant magnetic field  $\mathbf{H}$  inside the ferrofluid sample, the magnetization  $\mathbf{M}$ , and the externally applied magnetic field  $\mathbf{H}_0$  reads

$$\mathbf{H} + N\mathbf{M} = \mathbf{H}_0. \quad (1)$$

Here  $N$  denotes the demagnetizing factor that reflects the geometry of the sample under investigation ( $N=1/2$  in our experimental setup). Thus, to sum up, in a rotating ferrofluid a finite angle between  $\mathbf{H}$  and  $\mathbf{M}$  is formed when  $\mathbf{H}_0$  is perpendicular to the rotation axis.

## II. CHARACTERIZATION OF THE FERROFLUIDS

We used several ferrofluids out of the APG series of FerroTec. According to the manufacturer, the saturation magnetization of all the ferrofluids that we used is  $M_{\text{sat}}^{\text{FF}} = 17\,507$  A/m ( $\pm 10\%$ ) leading to a volume concentration  $\phi \approx 3.6\%$  of the suspended magnetic material. We have measured the equilibrium magnetization of the ferrofluids with a vibrating sample magnetometer (LakeShore 7300 VSM) with a commercial PC user package. In order to get information on the particle size distribution of the ferrofluid under investigation, we used a regularization procedure based on Tichonovs method [13]. Generally, the equilibrium magnetization  $M^{\text{eq}}(H)$  can be approximated by a superposition of Langevin-functions

$$M^{\text{eq}}(H) = \sum_{i=1}^N w_i \mathcal{L}[\alpha_i(H)]. \quad (2)$$

Here  $\mathcal{L}(x) = \coth(x) - 1/x$  denotes the Langevin function, which depends on the dimensionless Langevin parameter

$\alpha_i(H) = \mu_0 m_i H / k_B T$ , and  $w_i$  are the so-called magnetic weights.  $m_i$  refers to the magnetic moment of particles with magnetic diameter  $d_i$ , i.e.,  $m_i = \pi/6 d_i^3 M_{\text{sat}}^{\text{bulk}}$  with  $M_{\text{sat}}^{\text{bulk}}$  the bulk-saturation magnetization. From Eq. (2), we can deduce the initial susceptibility  $\chi_0 = (\pi \mu_0 M_{\text{sat}}^{\text{bulk}} / 18 k_B T) \sum_{i=1}^N w_i d_i^3$  and the saturation magnetization  $M_{\text{sat}}^{\text{FF}} = \sum_{i=1}^N w_i$  of the ferrofluid under investigation. Minimizing

$$\sigma = \sum_{i=1}^K [M^{\text{eq}}(H_k) - M_k]^2 \quad (3)$$

with respect to  $w_i$ , in which  $\{H_k, M_k\}_{k=1}^K$  indicate the experimental data, leads to an ill-posed problem, resulting in large positive and negative magnetic weights  $w_i$ . To avoid these unphysical results, one introduces an additional quantity  $\rho = \sum_{i=1}^N w_i^2$  and now minimizes

$$\sigma' = \sigma + \rho \tilde{\alpha} \quad (4)$$

with respect to  $w_i$ , where  $\tilde{\alpha}$  refers to the so-called regularization parameter ( $\tilde{\alpha}=0$  leads to the initial ill-posed problem). Using a small but finite positive  $\tilde{\alpha}$  allows for the computation of the distribution of the magnetic weights  $w_i$  as function of the particle diameters  $d_i$ .

In Fig. 1, we present the measured  $M^{\text{eq}}(H)$  curve together with the distribution of the magnetic weights  $w(d_i)$  (inset) for one of our sample ferrofluids. The solid curve was calculated using Eq. (2) together with  $w(d_i)$  as obtained from the regularization method. The solid line indicates the saturation magnetization of the ferrofluid sample with  $M_{\text{sat}}^{\text{FF}} = 19\,108.6$  A/m. From the saturation magnetization, the volume concentration of the magnetite particles was found to be  $\phi = M_{\text{sat}}^{\text{FF}} / M_{\text{sat}}^{\text{bulk}} = 4.1\%$ , in reasonable agreement with the manufacturer's specifications. For the initial susceptibility, we found the value  $\chi_0 = 1.09$ .

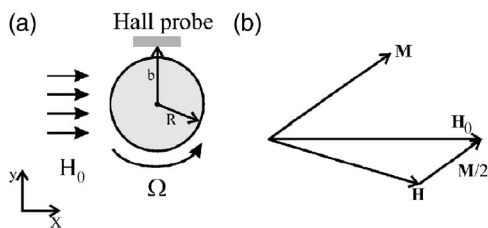


FIG. 2. Sketch of the experimental setup. (a) The cylindrical ferrofluid sample rotates with the angular velocity  $\Omega$  in the presence of the applied static magnetic field  $\mathbf{H}_0$  perpendicular to  $\Omega$ . The off-axis magnetization  $M_y$  is measured with a calibrated Hall probe located at the distance  $b=4.75$  mm from the middle of the cylindrical sample holder with inner radius  $R=3.2$  mm. (b) The fields  $\mathbf{M}$ ,  $\mathbf{H}$  within the ferrofluid sample.

### III. EXPERIMENTAL SETUP

The experimental setup is sketched in Fig. 2. The ferrofluid is filled into a cylindrical plexiglass sample holder with inside radius  $R=3.2$  mm. The sample is placed centrally between the poles of an electromagnet (Bruker B-E 10V) providing the homogeneous and temporally constant magnetic field  $\mathbf{H}_0=H_0\mathbf{e}_x$ . This field is constant within  $\pm 2\%$  in the spatial range of our experiment.

The cylindrical sample holder is mounted on an aluminum shaft, which is driven via a gearing system by a DC motor. The sample holder rotates with a constant rotation rate  $\Omega$ . The cylinder radius is so small that we can assume the flow  $\mathbf{u}$  always to be that of a rigid body, i.e.,  $\frac{1}{2}(\nabla \times \mathbf{u}) = \Omega \mathbf{e}_z$ .

The off-axis magnetization component  $M_y$  is measured by a Hall probe, mounted on an aluminum tube surrounding the sample and placed at the distance  $b=4.75$  mm away from the center of the cylindrical sample. According to the manufacturer's data sheet, the angular sensitivity range is  $\pm 3^\circ$ ; thus, the sensor responds only to field components perpendicular to the surface of the Hall sensor.

A Pt-100 resistor and a calibrated Gaussmeter (LakeShore 421 Gaussmeter) provide additional information about the experimental environment. The DC voltage for the motor and the magnet current are controlled by a LabView<sup>®</sup> program. The Hall voltage, Pt-100 resistance, rotation rate, and flux density are recorded by the program via a digital multimeter (Keithley 2000 multimeter) and an I/O card installed in a PC.

The magnetic field outside an infinitely long cylinder is given by

$$\mathbf{H}^{\text{out}} = \mathbf{H}_0 + \left(\frac{R}{r}\right)^2 \left(\frac{\mathbf{M} \cdot \mathbf{r}}{r} \frac{\mathbf{r}}{r} - \frac{1}{2}\mathbf{M}\right). \quad (5)$$

Here,  $R$  is the inner radius of the cylindrical fluid container,  $\mathbf{r}$  is the radial position vector, and  $\mathbf{H}_0$  is the externally applied magnetic field. Because of the finite size of the Hall sensor, the  $y$  component measured by the sensor is given by

$$H_y^{\text{sensor}} = \frac{1}{2a} \int_{-a}^a H_y^{\text{out}} dx = -\left(\frac{R}{\sqrt{a^2 + b^2}}\right)^2 H_y. \quad (6)$$

In our experimental setup,  $b=4.75$  mm,  $R=3.2$  mm, and  $a=2$  mm; here,  $a$  denotes the horizontal extension of the Hall

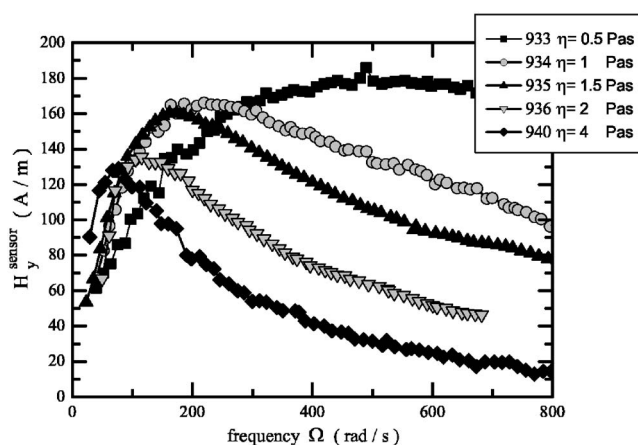


FIG. 3.  $H_y^{\text{sensor}}$  as function of  $\Omega$  at  $H_0=30$  kA/m for five ferrofluids out of the APG series of FerroTec that differ in their viscosity  $\eta$ .

sensor. With these values we find  $H_y^{\text{sensor}} = -0.386 H_y$ , where  $H_y = -M_y/2$  is the  $y$  component of the internal magnetic field in the ferrofluid.

### IV. EXPERIMENTAL RESULTS

#### A. Viscosity dependence

In the first experimental series, five ferrofluids with different viscosities were investigated. Our magnetogranulometric results confirmed the manufacturer's specification that the particle distributions were always the same. In each experiment of this series, the external magnetic field was  $H_0=30$  kA/m. We measured  $H_y$  as a function of  $\Omega$ , ranging from 0 up to 800 rad/s. The results of these measurements are presented in Fig. 3.

After completing the experiments at  $H_0=30$  kA/m, we performed the same measurements at  $H_0=15$  kA/m. In both experiments we observed a shift of the position of the maximum of the experimental curves toward lower  $\Omega$  values with increasing viscosity. This behavior reflects the Brownian nature of the relaxation process since the Néel process—the flip of the internal magnetic moment—is independent of the viscosity  $\eta$ . One can therefore expect that only Brownian particles, i.e., only those particles of sufficient size for the magnetic moment to be rigidly coupled to the crystalline structure of the particle, are capable of contributing to the transverse magnetization peak observed by our method.

From the position of the peak maximum, we deduced the relaxation time  $\tau$  via the relation  $\Omega^{\text{max}} \tau = 1 + \chi_0/2$ , suggested from a simple Debye approach ignoring the fact that here  $H_0$  was already too large to justify the use of the initial susceptibility  $\chi_0$ . In Fig. 4, we show the so-obtained relaxation time  $\tau$  as function of the fluid viscosity for two magnetic fields  $H_0=15$  kA/m and  $H_0=30$  kA/m, respectively. Note that the relaxation time for the former is larger by almost a factor 2 than the latter. This gives a first hint to the field dependence of the relaxation process. If one were to identify  $\tau$  by  $\tau^B = 3\eta V_h/k_B T$  with a hydrodynamic volume  $V_h = d_h^3 \pi/6$ , then one would obtain from the straight lines in Fig. 4 two differ-

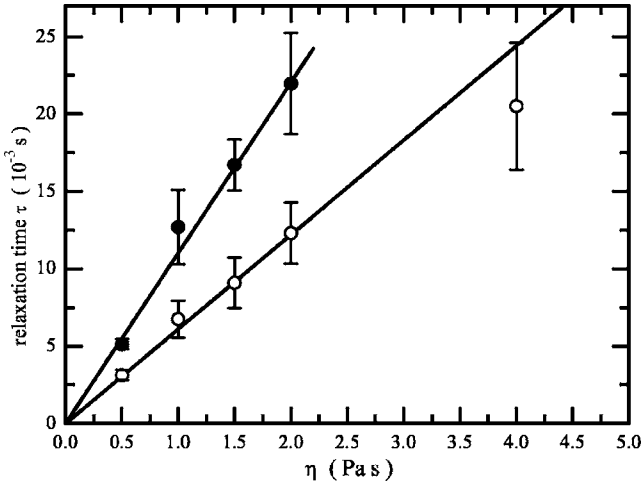


FIG. 4. Relaxation time  $\tau$  as function of the viscosity  $\eta$  given by the manufacturer. The relaxation time was determined using the relation  $\Omega^{\max}\tau = 1 + \chi_0/2$ , where  $\Omega^{\max}$  denotes the position of the maximum (cf. Fig. 3). Open circles denote measurements at  $H_0 = 30$  kA/m, full circles denote results of measurements performed at  $H_0 = 15$  kA/m. Error bars indicate the statistical errors.

ent estimates of the hydrodynamic particle diameters, namely,  $d_h = (25.0 \pm 1.7)$  nm from the data at  $H_0 = 30$  kA/m and  $d_h = (30.5 \pm 0.3)$  nm for  $H_0 = 15$  kA/m.

### B. Measurements at different constant external fields $H_0$

Further experiments that we describe in the remainder of this paper were performed on the ferrofluid APG 933 with  $\eta = 0.5$  Pa s. We measured  $H_y$  as a function of  $\Omega$  for a fixed value of  $H_0$ . After completing an experiment, we increased  $H_0$  and repeated the experiment. In this way, we got  $H_y(\Omega)$  for seven different values of  $H_0$ . The results of these measurements are shown in Fig. 5. One observes that the maximum amplitude of  $H_y$  increases with increasing  $H_0$  and that the peak position  $\Omega^{\max}$  is shifted toward higher  $\Omega$  values with increasing  $H_0$ .

In a first attempt to compare to theoretical models, we analyzed the experimental data obtained at  $H_0 = 30$  kA/m (cf. Fig. 7). To that end we calculated  $H_y^{\text{sensor}}(\Omega)$  numerically according to the models presented in the Appendix. In order to describe the experimental data with the theoretical models, we used  $\tau$  as fit parameter and, in addition, an *ad hoc* amplitude correction factor  $f$  (discussed below) which forces the model prediction for the maximal  $H_y^{\text{sensor}}$  to coincide with the measured one.

The fact that we found a much larger mean hydrodynamic diameter in the experiments with ferrofluids of different viscosities than in the equilibrium magnetization measurements and the necessity of an amplitude reduction factor  $f < 1$  reflects, in our opinion, the fact that only a fraction of the particles contribute to the experimental signal: only those particles contribute that have a volume large enough to ensure the magnetic moment to be fixed within the particle and therefore to relax in a Brownian manner. As already mentioned, there exist two distinct relaxation processes, namely, the Brownian and the Néel relaxation. Usually, one defines

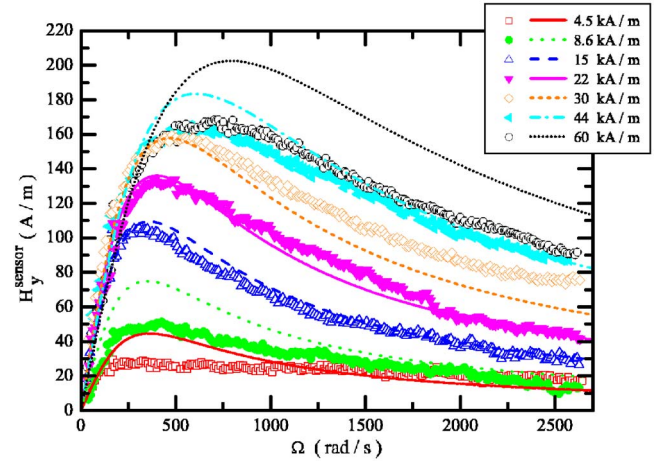


FIG. 5. (Color online) Comparison between the experimental data and the prediction of the Debye model with  $\tau(H)$  according to Eq. (8). Here the fit parameters  $\tau^B = 4$  ms,  $\gamma = 10^{-4}$  m/A, and  $f = 0.164$  were used.

the so-called effective relaxation time  $\tau^{\text{eff}}$  by the sum of two relaxation rates

$$\frac{1}{\tau^{\text{eff}}} = \frac{1}{\tau^B} + \frac{1}{\tau^N}. \quad (7)$$

Here,  $\tau^N = f_0^{-1} \exp(\kappa V_m / k_B T)$  is the Néel relaxation time ( $f_0$ : attempt frequency  $\sim 10^9$  Hz [14],  $\kappa$ : anisotropy constant,  $V_m$ : magnetic volume of the particle). The typical range of  $\kappa$  for magnetite-based ferrofluids is about 10–50 kJ/m<sup>3</sup> [15,16]. With, e.g.,  $\kappa = 44$  kJ/m<sup>3</sup>,  $\eta = 0.5$  Pa s,  $f_0 = 10^9$  Hz, and  $d_h = d_m + 2s$  with  $s = 2$  nm ( $s$  denotes the thickness of the polymeric surface layer), the Shliomis diameter  $d_S$ , at which  $\tau^B = \tau^N$ , was calculated to  $\approx 14$  nm. Therefore, only particles with a diameter  $d > d_S$  relax via the Brownian process and contribute to the observed phenomenon. In Fig. 6,  $\tau^B$ ,  $\tau^N$ , and  $\tau^{\text{eff}}$  are plotted for  $\kappa_1 = 44$  kJ/m<sup>3</sup>,  $\kappa_2 = 11$  kJ/m<sup>3</sup>,  $\eta = 0.5$  Pa s,  $f_0 = 10^9$  Hz, and  $s = 2$  nm. For  $\kappa_1 = 44$  kJ/m<sup>3</sup>, the Shliomis diameter is  $d_S \approx 14$  nm, whereas for  $\kappa_2 = 11$  kJ/m<sup>3</sup>,  $d_S \approx 23$  nm. This indicates a strong influence of the anisotropy constant  $\kappa$  on the boundary between large particles that relax via the Brownian process, that therefore, contribute to the observed phenomenon, and those that relax in a Néelian way.

### Theoretical modeling

As mentioned already, in our first attempt to describe the behavior of the magnetization  $\mathbf{M}$  for rotating ferrofluids, we used the single-relaxation-time models listed in the Appendix. They are discussed at greater length in Ref. [17]. Figure 7 shows comparisons of experimental data with the fits for the case of the medium-sized field  $H_0 = 30$  kA/m. The parameters used to calculate  $H_y(\Omega)$  are summarized in Table I.

We found that the models FK, S'01, and S'72 with the finite  $\alpha_3 = \mu_0 / 4\zeta$  do not properly reproduce the position  $\Omega^{\max}$  of the maximum of the experimental curve in Fig. 7. In fact, expression (A9) shows that the initial slope for the models with  $\alpha_3 = \mu_0 / 4\zeta$  is primarily determined by the external field value  $H_0$ . Therefore, even a substantial increase of  $\tau$  would

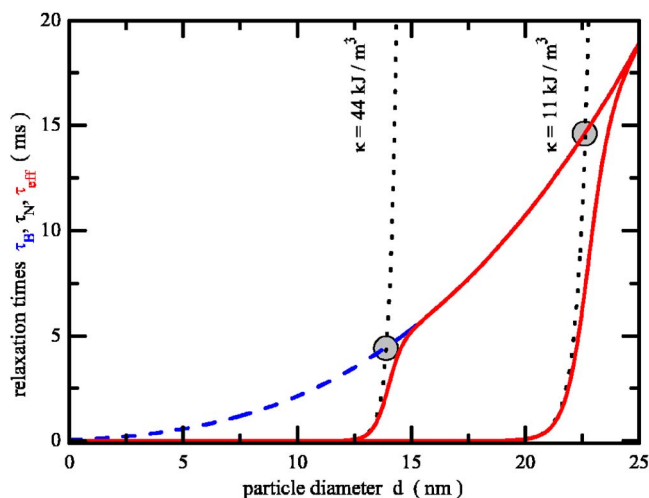


FIG. 6. (Color online) Illustration of the relaxation times  $\tau^B$ ,  $\tau^N$ , and  $\tau^{\text{eff}}$  as function of the magnetic particle diameter in nanometers. The dashed curve corresponds to the Brownian relaxation time  $\tau^B$ . The dotted curves represent relaxation times according to Néel for two different  $\kappa_1=44 \text{ kJ/m}^3$  and  $\kappa_2=11 \text{ kJ/m}^3$ . The solid curves show the effective relaxation times. The intersections of  $\tau^B=\tau^N$  are marked with gray circles.

shift the curves only slightly to smaller  $\Omega$ . Another drawback of the FK, S'01, and S'72 models is that the slope of the curves becomes more and more negative for  $\Omega > \Omega^{\text{max}}$ . In contrast, using the models with  $\alpha_3=0$  with an appropriate choice of the fit parameter  $\tau$ , we can reproduce the peak position  $\Omega^{\text{max}}$ . However, only the model ML(S) reproduces the experimental curve in Fig. 7 for larger values of  $\Omega$ .

From the measured curves of  $H_y(\Omega, H_0)$  vs  $H_0$ , we extracted the position of the maximum [denoted as  $\Omega^{\text{max}}(H_0)$ ] and the maximum value  $\max(H_y^{\text{sensor}})=H_y^{\text{sensor}}(\Omega^{\text{max}}, H_0)$ . The latter is shown in Fig. 8 in comparison to the results of the models. In order to fit the maximum amplitude, we had to introduce an *ad hoc* additional amplitude reduction factor  $f$  (cf. Table I). Note that the models Debye and S'72 yield the

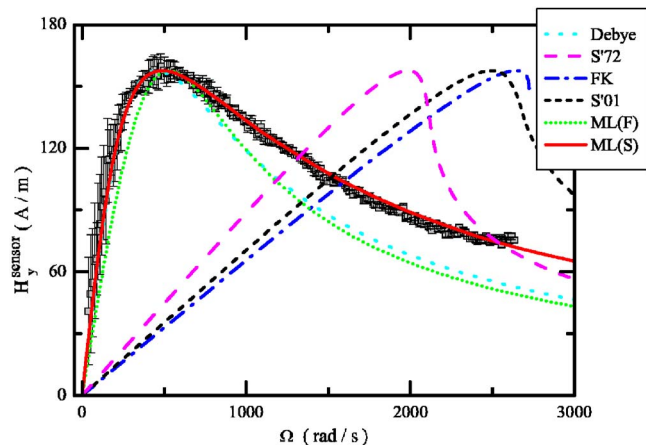


FIG. 7. (Color online) Comparison of the experimental data (symbols) obtained at  $H_0=30 \text{ kA/m}$  with the numerical results according to different theoretical models (cf. Appendix). See Table I for an identification of the curves and the fit parameters used.

TABLE I. Models described in the Appendix are used in Fig. 7 in order to get the presented curves.  $f$  factor refers to the amplitude factor.

Model	Color	$f$ factor	Relaxation time $\tau$ (ms)
Debye	cyan	0.164	2.5
S'72	magenta	0.164	2.5
FK	blue	0.125	5
S'01	black	0.125	3.5
ML(F)	green	0.125	6
ML(S)	red	0.125	3.5

same maximum [17]. The other models [FK, S'01, ML(F), and ML(S)] also have a common but different maximal  $H_y$ . Thus, Table I contains only two different amplitude reduction factors  $f$ . Figure 8 shows that, already, the simple Debye model reasonably well reproduces the variation of  $\max(H_y^{\text{sensor}})$  with  $H_0$  if one ignores the *ad hoc* amplitude reduction factor.

We mentioned above that the models with  $\alpha_3 \neq 0$  do not reproduce the experimental peak positions  $\Omega^{\text{max}}$ . Figure 9(a) shows  $\Omega^{\text{max}}$  as function of  $H_0$  compared to numerical results of Debye and ML. Debye yields a shift in the wrong direction, while the peak positions of ML(S) do not increase strongly enough with increasing  $H_0$ . On the other hand, the ML(F) results show a somewhat better agreement with the experimental data.

We also mentioned that the simple Debye model yields better values for the amplitude  $\max(H_y^{\text{sensor}})$ . Thus, in order to describe both the variation of the amplitude  $\max(H_y^{\text{sensor}})$

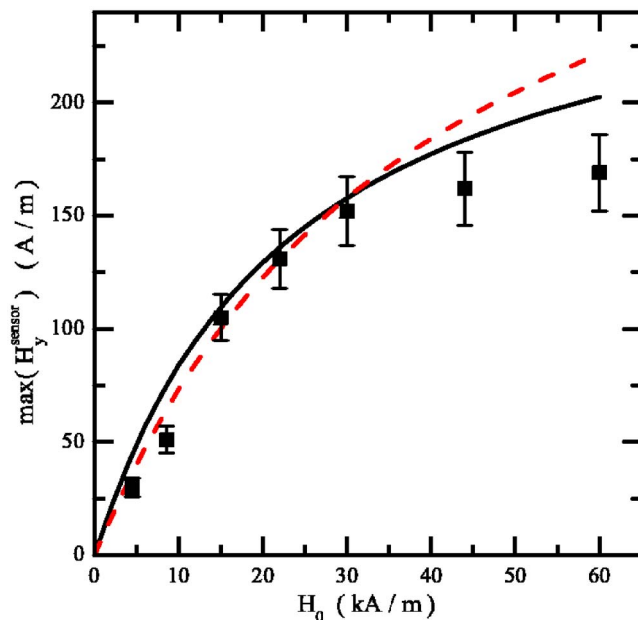


FIG. 8. (Color online) Maxima of  $H_y^{\text{sensor}}=H_y^{\text{sensor}}(\Omega^{\text{max}})$  as a function of the external field  $H_0$ . Squares with error bars refer to experimental data. Solid line shows the result of the Debye and S'72 model. Dashed line is common to the models denoted as FK, S'01, and ML. Parameters are listed in Table I.

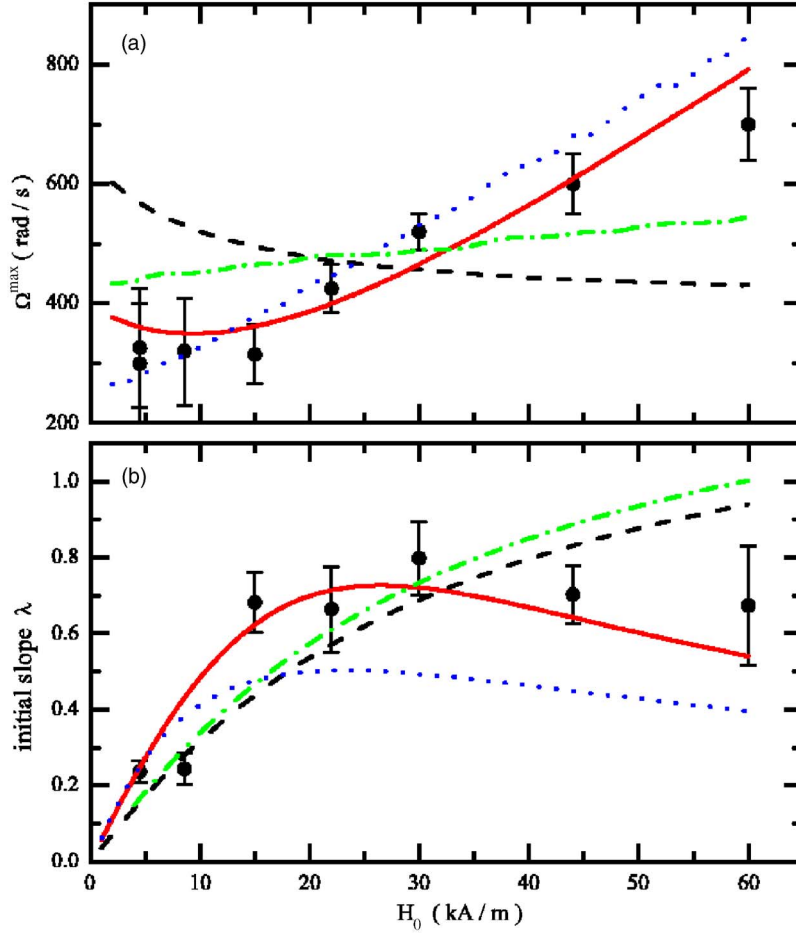


FIG. 9. (Color online) (a) maxima locations,  $\Omega^{\max}$ , and (b) initial slopes,  $\lambda$  (9), of the curves  $H_y^{\text{sensor}}(\Omega, H_0)$  vs  $H_0$ . Circles with error bars: experiments. Dashed lines: simple Debye model with  $\tau=2.5$  ms,  $f=0.164$ . Dotted lines: ML(F) with  $\tau=6$  ms,  $f=0.125$ . Dashed-dotted lines: ML(S) with  $\tau=3.5$  ms,  $f=0.125$ . Full lines: generalized Debye model with  $\tau(H)$  according to Eq. (9) and  $\tau^B=4$  ms,  $\gamma=10^{-4}$  m/A,  $f=0.164$ .

with  $H_0$  as well as the obvious increase of  $\Omega^{\max}$  with the magnetic field, we finally used the Debye model with an  $H$ -dependent relaxation rate  $1/\tau(H)$  that increases with  $H$  according to the simple relaxation time ansatz [18]

$$\tau(H) = 2\tau^B \frac{\mathcal{L}(\alpha)}{\alpha - \mathcal{L}(\alpha)}. \quad (8)$$

Here  $\tau^B$  denotes the Brownian relaxation time,  $\mathcal{L}(\alpha)$  is the already-mentioned Langevin function, and  $\alpha = \gamma H$ . For this generalized Debye model, we used  $\tau^B$  and  $\gamma$  as fit parameters together with the amplitude reduction factor  $f=0.164$  obtained for the simple Debye model.

We also analyzed the behavior of our experimental curves in the low-frequency regime, i.e., the initial slope

$$\lambda = \left. \frac{dH_y^{\text{sensor}}}{d\Omega} \right|_{\Omega \rightarrow 0} \quad (9)$$

as a function of  $H_0$ . For a quantitative evaluation of the experimental  $\lambda$ , we need to determine the linear frequency region for each  $H_0$  separately. This is accomplished with a linear regression fit with error weighting. The basic idea of that method is to minimize the so-called  $\xi$ -square merit function

$$\xi^2 = \frac{1}{N_d} \sum_{i=1}^{N_d} \left( \frac{H_y^{(i)} - \chi \Omega^{(i)}}{\Delta H_y^{(i)}} \right)^2 \quad (10)$$

so as to get  $\chi$  and its error bar [19]. Here  $\Delta H_y^{(i)}$  is the error bar related to the measured data of  $H_y^{(i)}$ . In Fig. 9(b), we show the experimental initial slope  $\lambda$  as a function of  $H_0$  in comparison to model predictions; again the Debye model with  $H$ -dependent relaxation time  $\tau$  represents the experimental data best.

## V. DISCUSSION AND CONCLUSION

The results of Figs. 9(a) and 9(b) can be summarized as follows: ML(F) with  $\tau \approx 6$  ms and  $f=0.125$  (dotted lines) reproduces the behavior of  $\Omega^{\max}$  and the initial slope  $\lambda$  (9) quite reasonably, whereas the simple Debye model with a constant  $\tau=3.5$  ms and  $f=0.164$  (dashed lines) is inferior, in particular, because of the shift of  $\Omega^{\max}$  in the wrong direction. The generalized Debye model with the  $H$ -dependent  $\tau(H)$  (8) and  $\tau^B=4$  ms,  $\gamma=10^{-4}$  m/A, and  $f=0.164$  (full lines) reproduces  $\Omega^{\max}$  and  $\lambda$  significantly better than the simple Debye model. As an aside, we mention that, in using the simple Debye model with other combinations of  $\tau^B$ ,  $\gamma$  one can get reasonable values of  $\Omega^{\max}$  as well while the initial slope  $\lambda$  depends more sensitively on these parameters. The models FK, S'01, and S'72 with the nonlinear contribu-

tions  $\alpha_3[\mathbf{M} \times (\mathbf{M} \times \mathbf{H}_0)]$  to the relaxation of the magnetization were not included in Figs. 9 since their predictions for  $H_y(\Omega, H_0)$  are for larger  $H_0$  too far off from the experimental results (cf, e.g., Fig. 7). With this reasoning, we tried to fit our complete set of data of Fig. 5 at different  $H_0$  consistently with the extended Debye model, but the quality of the data reproduction is rather limited because of the substantial deviations at small and large  $H_0$ .

For the above-obtained parameter  $\tau^B=4$  ms, the hydrodynamic particle diameter would be  $d_h \approx 27.5$  nm. This again supports the argument that the observed  $H_y$  is produced only by the large particles.

Heegaard *et al.* [7] used a ferrofluid containing cobalt ferrite particles, and the viscosity of the fluid is given as  $\eta = 1$  Pa s. They found a Brownian relaxation  $\tau^B=6$  ms; assuming spherical particles, this relaxation time is correlated to a hydrodynamic diameter of about  $d_H \approx 30$  nm, whereas the characteristic magnetic size is  $d_m=8.2$  nm. The relaxation time obtained in Ref. [7] is comparable to the relaxation time  $\tau^B=4$  ms that was inferred from our experiments using the generalized Debye model. The large Brownian relaxation time implicates the presence of large particles or even clusters within the fluid.

Lal *et al.* [20] used x-ray photon correlation spectroscopy in order to study the static and dynamic behavior of ferrofluids. These authors investigated a ferrofluid containing maghemite particles ( $\gamma\text{-Fe}_3\text{O}_4$ ) with a volume concentration of  $\phi=3.5\%$ . From the measured autocorrelation functions  $g(t)$ , they extracted the relaxation rates  $\Gamma(Q)$  as a function of  $Q^2$ . A fit to their data yields a diffusion coefficient  $D_0=9.1 \times 10^{-10}$  cm<sup>2</sup>/s. With the help of the Stokes-Einstein relation,

$$D_0 = 6\pi\eta R_H/k_B T \quad (11)$$

and  $\eta=0.4$  Poise, the hydrodynamic radius was found to be  $R_H=591$  Å, i.e., the diffusing object (observed for  $Q < 0.01$  Å<sup>-1</sup>) is much bigger than the individual colloidal sphere with a nominal radius of  $r \approx 80$  Å.

In this paper, we have presented measurements of the transverse magnetization of a ferrofluid rotating as a rigid body in the presence of a static magnetic field oriented perpendicular to the axis of rotation. The rotation rates extend well into the range of  $\Omega\tau > 1$ . For the largest magnetic fields, the equilibrium magnetization already shows significant deviations from a linear behavior.

The comparison of our experimental results with the predictions of several different models can be summarized as follows: Models S'72, S'01, and FK have a tendency to shift the maximal location  $\Omega_{\max}$  in the transverse magnetization, i.e., in the curves of  $H_y(\Omega)$  to frequencies that are too large in comparison to experiments. Furthermore, the shape of the curves for  $H_y(\Omega)$  vs  $\Omega$  are somewhat better reproduced by the ML and Debye models. Concerning the variation of the maximum location  $\Omega_{\max}$  of  $H_y$  and of its low-frequency slope ( $dH_y/d\Omega$ ) with externally applied field  $H_0$ , we found that ML(S) and a simple Debye model are inferior to ML(F) and a Debye model with a field-dependent relaxation rate  $\tau(H)$  with the latter lying slightly closer to experiments than the former. But none of these single-relaxation-time models

TABLE II. Coefficients in Eqs. (A1)–(A7). Here  $\chi=\chi(H) = M^{\text{eq}}(H)/H$  denotes the chord susceptibility,  $\tau$  is the relaxation time, and  $F=F(M)$  is the inverse function of  $M^{\text{eq}}(H)$  divided by  $M$ . Furthermore,  $\mu_0=4\pi \times 10^{-7}$  Vs/Am and  $\zeta=3/2\phi\eta$  (vortex viscosity) with the volume fraction  $\phi$ .

Model	$\alpha_1$	$\alpha_2$	$\alpha_3$	Eq.
Debye <sup>a</sup>	$\chi/\tau$	$1/\chi+1/2$	0	(A1)
S'72 <sup>b</sup>	$\chi/\tau$	$1/\chi+1/2$	$\mu_0/4\zeta$	(A2)
FK <sup>c</sup>	$\gamma_H$	$F+1/2$	$\mu_0/4\zeta$	(A4)
S'01 <sup>d</sup>	$1/(F\tau)$	$F+1/2$	$\mu_0/4\zeta$	(A3)
ML <sup>e</sup>	$\xi$	$F+1/2$	0	(A5)

<sup>a</sup>Reference [1].

<sup>b</sup>Reference [21].

<sup>c</sup>Reference [22].

<sup>d</sup>Reference [23].

<sup>e</sup>Reference [24].

seems to describe our findings in the full range of frequencies and external magnetic fields and all of them require a substantial overall amplitude reduction factor since their predictions concerning the magnitude of the transverse magnetization are too large by factors of 6–8 (these  $f$  factors are summarized in Table I). Furthermore, they do not properly describe the experimentally observed saturation behavior of  $H_y^{\text{sensor}}(\Omega)$  with increasing  $H_0$ .

Real ferrofluids, being composed of a broad distribution of particles sizes, presumably show more complex magnetization dynamics than those of the models here, in particular, when  $\Omega$  is not very small compared to the smallest relaxation rate of the system. In semidilute systems, where the dipolar interaction between the magnetic particles is not yet relevant, one can expect the magnetic degrees of freedom to relax independently from each other. We are currently investigating such polydisperse model extensions to describe the experimental data.

## ACKNOWLEDGMENTS

This work was supported by the DFG (Grant No. SFB 277) and the INTAS (Grant No. 03-51-6064). Discussions with K. Knorr are gratefully acknowledged. We thank J. Albers for contributions to an earlier version of the experimental setup.

## APPENDIX: MODELS

The model equations for the magnetization in situations where  $\mathbf{M}$  and  $\mathbf{H}$  are spatially and temporally constant but not parallel to each other include either a term describing the relaxation of  $\mathbf{M}$  toward  $\mathbf{M}^{\text{eq}}(\mathbf{H})$  or of the effective field  $\mathbf{H}^{\text{eff}}(\mathbf{M})$  toward the internal magnetic field  $\mathbf{H}$  [17]. We consider here five different models (Table II) that are discussed in Ref. [17]. They yield the following relations between the fields

$$\text{Debye [1]: } \quad \Omega \times \mathbf{M} = \frac{1}{\tau}(\mathbf{M} - \mathbf{M}^{\text{eq}}) \quad (A1)$$

$$S'72 [21]: \quad \boldsymbol{\Omega} \times \mathbf{M} = \frac{1}{\tau}(\mathbf{M} - \mathbf{M}^{\text{eq}}) + \frac{\mu_0}{4\zeta}[\mathbf{M} \times (\mathbf{M} \times \mathbf{H})] \quad (\text{A2})$$

$$\text{FK [22]:} \quad \boldsymbol{\Omega} \times \mathbf{M} = \gamma_H(\mathbf{H}^{\text{eff}} - \mathbf{H}) + \frac{\mu_0}{4\zeta}[\mathbf{M} \times (\mathbf{M} \times \mathbf{H})] \quad (\text{A3})$$

$$S'01 [23]: \quad \boldsymbol{\Omega} \times \mathbf{H}^{\text{eff}} = \frac{1}{\tau}(\mathbf{H}^{\text{eff}} - \mathbf{H}) + \frac{\mu_0}{4\zeta}[\mathbf{H}^{\text{eff}} \times (\mathbf{M} \times \mathbf{H})] \quad (\text{A4})$$

$$\text{ML [24]:} \quad \boldsymbol{\Omega} \times \mathbf{M} = \xi(\mathbf{H}^{\text{eff}} - \mathbf{H}). \quad (\text{A5})$$

They are solved numerically together with the relation

$$\mathbf{H} = \mathbf{H}_0 - \mathbf{M}/2, \quad (\text{A6})$$

following from Maxwell's equations. Note that  $H_y = -M_y/2$  for our setup. As outlined in Ref. [17], the equations can be written in the following common form:

$$\boldsymbol{\Omega} \times \mathbf{M} = \alpha_1(\alpha_2 \mathbf{M} - \mathbf{H}_0) + \alpha_3[\mathbf{M} \times (\mathbf{M} \times \mathbf{H}_0)] \quad (\text{A7})$$

with the coefficients summarized in Table II. For  $\gamma_H$ , we used  $\gamma_H = \chi_0/\tau$  [22]. For the parameter  $\xi$ , we investigated two different choices: either the low-field variant,  $\xi = \chi_0/\tau$  as in Ref. [22]; which is denoted here by ML(F), or the variant  $\xi = 1/[F(M)\tau]$  as in Ref. [23], which is referred to as ML(S).

Performing an expansion for small  $\Omega$ , we obtained from Eq. (A7) an expression for  $M_y$  of first order in  $\Omega$

$$M_y^{(1)} = \frac{M_{\text{eq}}^2}{\alpha_1 + \alpha_3 M_{\text{eq}}^2} \frac{\Omega}{H_0}. \quad (\text{A8})$$

From this equation, we find for the initial slope the relation

$$\left. \frac{dM_y}{d\Omega} \right|_{\Omega \rightarrow 0} = \frac{M_y^{(1)}}{\Omega} = \frac{M_{\text{eq}}^2}{\alpha_1 + \alpha_3 M_{\text{eq}}^2} \frac{1}{H_0}. \quad (\text{A9})$$

- 
- [1] R. E. Rosensweig, *Ferrohydrodynamics* (Cambridge University Press, Cambridge, England, 1985).
- [2] J. P. McTague, *J. Chem. Phys.* **51**, 133 (1969).
- [3] M. I. Shliomis, *Sov. Phys. JETP* **34**, 1291 (1972).
- [4] M. I. Shliomis and K. I. Morozov, *Phys. Fluids* **6**, 2855 (1994).
- [5] J. C. Bacri, R. Perzynski, M. I. Shliomis, and G. I. Burde, *Phys. Rev. Lett.* **75**, 2128 (1995).
- [6] A. Zeuner, R. Richter, and I. Rehberg, *Phys. Rev. E* **58**, 6287 (1998).
- [7] B. M. Heegaard, J.-C. Bacri, R. Perzynski, and M. I. Shliomis, *Europhys. Lett.* **34**, 299 (1996).
- [8] F. Gazeau, C. Baravian, J. C. Bacri, R. Perzynski, and M. I. Shliomis, *Phys. Rev. E* **56**, 614 (1997).
- [9] C. Alexiou, *Cancer Res.* **60**, 6641 (2000).
- [10] C. Alexiou, *J. Drug Target.* **11**, 129 (2003).
- [11] F. Gazeau, B. M. Heegaard, J.-C. Bacri, A. Cebers, and R. Perzynski, *Europhys. Lett.* **35**, 609 (1996).
- [12] J. Embs, H. W. Müller, C. Wagner, K. Knorr, and M. Lücke, *Phys. Rev. E* **61**, R2196 (2000).
- [13] T. Weser and K. Stierstadt, *Z. Phys. B: Condens. Matter* **59**, 253 (1985).
- [14] T. K. McNab, R. A. Fox, and J. F. Boyle, *J. Appl. Phys.* **39**, 5703 (1968).
- [15] P. C. Fannin, P. A. Preov, and S. W. Charles, *J. Phys. D* **32**, 1583 (1999).
- [16] P. C. Fannin, *J. Magn. Magn. Mater.* **136**, 49 (1994).
- [17] A. Leschhorn and M. Lucke, *Z. Phys. Chem.* **220**, 219 (2006).
- [18] M. A. Martsenyuk, Y. L. Raihker, and M. I. Shliomis, *Sov. Phys. JETP* **38**, 413 (1974).
- [19] Z. Wang, C. Holm, and H. W. Müller, *Phys. Rev. E* **66**, 021405 (2002).
- [20] J. Lal, D. Abernathy, L. Auvray, O. Diat, and G. Grübel, *Eur. Phys. J. E* **4**, 263 (2001).
- [21] M. I. Shliomis, *Sov. Phys. JETP* **34**, 1291 (1972).
- [22] B. U. Felderhof and H. J. Kroh, *J. Chem. Phys.* **110**, 7403 (1999).
- [23] M. I. Shliomis, *Phys. Rev. E* **64**, 060501(R) (2001).
- [24] H. W. Müller and M. Liu, *Phys. Rev. E* **64**, 061405 (2001).